Anisotropy and crystal plasticity study of fcc polycrystalline Ni by nanoindentation

Emile Renner, Patrick Delobelle, Yves Gaillard, Fabrice Richard

Anisotropy and crystal plasticity study of fcc polycrystalline Ni by nanoindentation

E. Renner, P. Delobelle, Y. Gaillard, F. Richard

Département Mécanique Appliquée (DMA), FEMTO-ST, CNRS UMR 6174/UFC/ENSMM/UTBM, Université de Franche-Comté, 24 rue de l'Epitaphe, 25000 BESANCON

Résumé :

L'objectif de l'étude est de mettre en lumière l'anisotropie des matériaux cristallins de type cfc aux échelles micro et nanométriques. Des résultats numériques et expérimentaux de nanoindentation sont présentés. Les essais expérimentaux ont été réalisés sur un échantillon de nickel polycristallin, avec un indenteur de type Berkovich. Les simulations ont été menées sous le code éléments finis ZEBULON, en y intégrant un modèle de plasticité cristalline en grande déformation. Trois directions cristallographiques principales, correspondant à trois grains présentant ces mêmes directions, ont été choisies comme axe d'indentation, à savoir [001], [101] et [111]. Les empreintes ont été analysées au microscope à force atomique (AFM). La topographie de la surface autour des empreintes a révélé des lignes de glissement associées aux différents systèmes activés, ainsi que des remontées de matière (bourrelets) fortement anisotropes et non-symétriques, dépendantes de l'orientation du cristal par rapport à l'indenteur. Ces observations sont en accord avec les résultats des simulations numériques. L'effet de l'orientation de l'indenteur dans chacun des plans d'indentation a également été étudié expérimentalement et numériquement.

Abstract :

The goal of the study is to probe the anisotropy of fcc grain of polycrystalline material at the micro and nano-scales. Numerical and experimental results of nanoindentation are reported. The tests were conducted on bulk polycrystalline nickel with a Berkovich indenter. The finite element code ZEBULON, in which a large deformation crystal plasticity constitutive model is implemented, was used for the simulations. Three main crystallographic directions, corresponding to three grain orientations, were chosen as indentation axis, i.e. [001], [101] and [111]. Indentation imprints were analyzed thanks to an atomic force microscope (AFM). The surface topography around the indents has revealed slip traces associated to the different activated systems and pile-up which are strongly anisotropic and asymmetric, depending on the crystal orientation. These observations are in a good agreement with the simulation results. The role of the indenter orientation for each indentation plane was also examined experimentally and numerically.

Keywords : Nanoindentation, Anisotropy, Crystal plasticity, Finite element analysis

1 Introduction

In the last decades, instrumented indentation has become an efficient tool to analyze at micro and nanoscales mechanical properties of materials, such as hardness and elastic modulus. Furthermore, pile-up analysis can also be used for investigating anisotropy and plasticity. Indeed, numerous works have shown that pile-up directly depends on material properties (Holmes [1], Stelmashenko [2], Nibur [3], McElhaney [4], Wang [5]). They are thus precious information sources and may even be considered as a fingerprint of the studied material.

Finite element modelings of nanoindentation test are very powerful for analysis and give a lot of post-treatment possibilities. In the single crystal context, 3D finite element modeling of nanoindentation test has been conducted during the last decade (Wang [5], Liu [6], Casals [7], Zambaldi [8], Eidel [9]).

To account for the mechanical behavior of single crystal, constitutive models have been developed around Hill & Rice [10] works and have been implemented in finite element softwares. In the present study, Méric-Cailletaud single crystal plasticity model [11] is used with the ZEBULON code.

2 Experimental protocol and material

2.1 Material

The experimental part makes use of an annealed polycrystalline nickel sample nickel ($\emptyset_{mean}$~140 μm). Nickel is a fcc material with an anisotropic coefficient $f = 2C_{44}/(C_{11} - C_{12}) = 2{,}44$. EBSD measurements gave a map of grain orientations in the studied zone. The sample was chemically etched and then carefully polished with colloidal alumina before indenting.

2.2 Experimental conditions

A NHT CSM indenter system was used for indentation tests at room temperature. The indenter is a Berkovich diamond tip (triangular based pyramid). The indentations are controlled in load and the maximum value is set to 30 mN, corresponding to indentation depths of about 800-900 nm. Thanks to EBSD measurements, it was possible to perform indentations in three different crystallographic planes belonging to the following family of lattice planes : {001}, {101} and {111} (Figure 1). To study the indenter orientation effects in each indentation planes, the sample was successively rotated of 30° and 60°. For each indentation direction and indenter orientation, three indentations have been made in order to assess the repeatability of the results

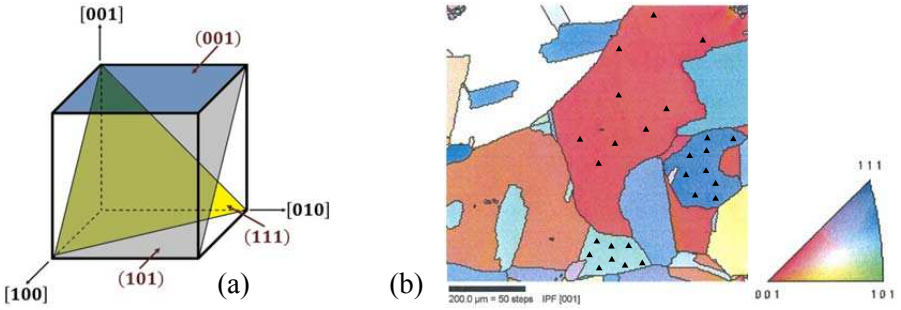

FIG. 1 – (a) Schematic view of the three crystallographic planes indented (001), (101) and (111) (b) EBSD measurements of the studied zone and indentation positions.

3 Numerical simulations

3.1 Single crystal plasticity constitutive equations

Due to the large grain size, each indented grain can be considered as a single crystal with a defined orientation. Simulations were conducted in the large deformation framework. An elastic tensor was considered to model the single crystal elastic response. The Méric-Cailletaud single crystal plasticity model [11] was used to describe the viscoplastic behavior. The transformation gradient is decomposed as follows:

$$\bar{\bar{F}} = \overline{\overline{F^e}}\ \overline{\overline{F^p}} \tag{1}$$

where $\overline{\overline{F^e}}$ is the transformation gradient due to elastic strain and lattice rotation. In the fcc single crystal plasticity framework, $\overline{\overline{F^p}}$ is the transformation gradient due to plastic shear strain in each of the 12 slip systems $\overline{\overline{m^s}}$, defined by the normal vectors of the slip planes $\overline{n^s}$ and the slip directions $\overline{l^s}$.

$$\dot{\overline{\overline{F^p}}}\ \overline{\overline{F^p}}^{-1} = \sum_{s=1}^{12} \dot{\gamma^s}\ \overline{\overline{m^s}}\ \ with\ \ \overline{\overline{m^s}} = \overline{l^s} \otimes \overline{n^s} \tag{2}$$

The resolved shear stress on each slip systems is given by:

$$\tau^s = \overline{\overline{m^s}} : \bar{\bar{\sigma}} \tag{3}$$

The inelastic flow is governed by a Norton power law:

$$\dot{\gamma^s} = \left\langle \frac{|\tau^s - x^s| - r^s}{K} \right\rangle^n sign(\tau^s - x^s), with\ \langle \bullet \rangle = \begin{cases} \bullet\ if \bullet > 0 \\ 0\ \ if \bullet < 0 \end{cases} \tag{4}$$

where n and K are viscosity parameters. The hardening has been considered as kinematic and isotropic through the x^s and r^s variables, respectively.

$$\dot{x^s} = C\dot{\gamma^s} - D\left|\dot{\gamma^s}\right|x^s \tag{5}$$

$$r^s = R_0 + Q\sum_{r=1}^{12} h^{sr}\left[1 - \exp(-bv^r)\right], with\ \dot{v^r} = \left|\dot{\gamma^r}\right| \tag{6}$$

C, D, b and Q are material parameters. R_0 is the critical resolved shear stress of slip systems. $h^{sr}$is the interaction matrix (12x12 components) where diagonal terms define self-hardening and off-diagonal terms define latent hardening.

3.2 Finite element modeling

Numerical simulations of nanoindentation test were conducted using the finite element code ZEBULON. The indentation is performed on a cylinder whose radius and height are 36 µm. The maximal indentation depth is 900 nm, that is one fortieth of the cylinder height. One can thus impose the lower cylinder surface to be clamped. Lateral surfaces are free and the Berkovich indenter, which is considered as rigid, is controlled in displacement along the $\vec{Z}$ indentation axis and locked along the other ones. The mesh is refined near the contact region. Figure 2 summarizes the modeling conditions. Simulations have been conducted in 3D to account for anisotropy.

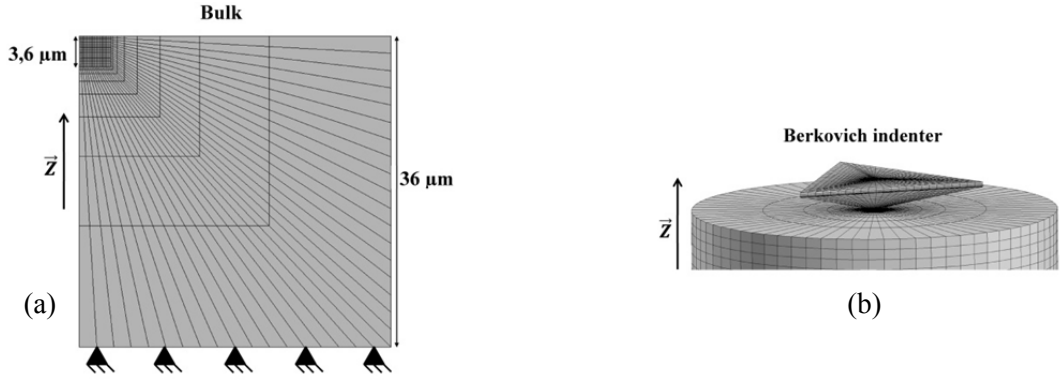

FIG. 2 – Modeling boundary conditions and mesh details: bulk (a), Berkovich indenter (b).

Elastic material parameters are set to $C_{11} = 248$ GPa, $C_{12} = 153$ GPa, $C_{44} = 116$ GPa and all the h^{sr} coefficients have been taken as unity (h^{sr}=1). The present work is anyway intended to provide qualitative description of the surface deformation around the indentation imprint. The number and orientation of pile-up depend on the material crystallography and on the activated slip systems. Except for the h^{sr} coefficients, the values of the different model parameters have thus no effect on the symmetry of the observed tendencies. Even though the same slip systems are experimentally and numerically activated, the pile-up dimensions (height, width) will not be compared because they strongly depend on the plasticity parameters introduced in the constitutive laws.

4 Results and discussion

According to the material crystallography, the evacuation of the material excess at the sample surface around the indenter takes place along precise directions and thus results in pile-up. The distribution of these piles-up at precise locations around the imprint has been studied by Holmes [1], Wang [5] and Eidel [10] on Y_2O_3-stabilized cubic ZrO_2, copper and Ni-base superalloy, respectively.

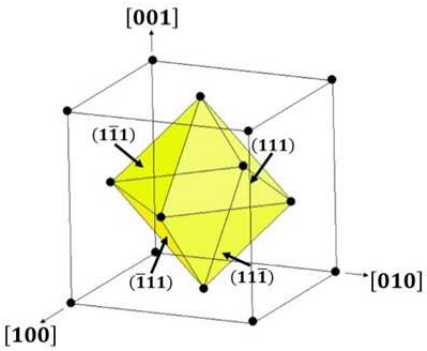

FIG. 3 – Octahedral slip systems in a fcc crystal.

At room temperature, for fcc single crystal metals, the inelastic flow occurs in the octahedral slip systems (Figure 3), namely $\{111\}\langle 110\rangle$. When the indentation is conducted in the [001] direction, four piles-up are formed along the $[110], [\bar{1}10], [1\bar{1}0]$ and $[\bar{1}\bar{1}0]$ directions involving a four-fold symmetry. In the [101] indentation direction, matter flows and piles-up occur along the $[12\bar{1}]$,$[\bar{1}21]$, $[\bar{1}2\bar{1}]$ and $[1\bar{2}\bar{1}]$ directions, resulting in a two-fold symmetry. Finally, when the indentation is performed in the [111] direction, six piles-up are susceptible to appear along the $[\bar{1}10]$, $[\bar{1}01]$, $[0\bar{1}1]$, $[1\bar{1}0]$, $[10\bar{1}]$ and $[01\bar{1}]$ directions, describing a six-fold symmetry. These remarks are valid in the context of axisymmetric indentation, the use of a Berkovich indenter will promote certain directions instead of another.

After analyzing the AFM measurements of the different configurations, one can notice that the propagation directions of the pile-up are the intersection directions between the $\{111\}$ family planes and the indentation plane. A definition of the pile-up propagation directions for fcc single crystals metals is proposed as follows:

$$[x, y, z] = \{\{111\} \cap (i, j, k)\} \tag{7}$$

with (i,j,k) the plane whose normal vector is the indentation direction.

The Figure 4 illustrates the foregoing for the three indentation directions.

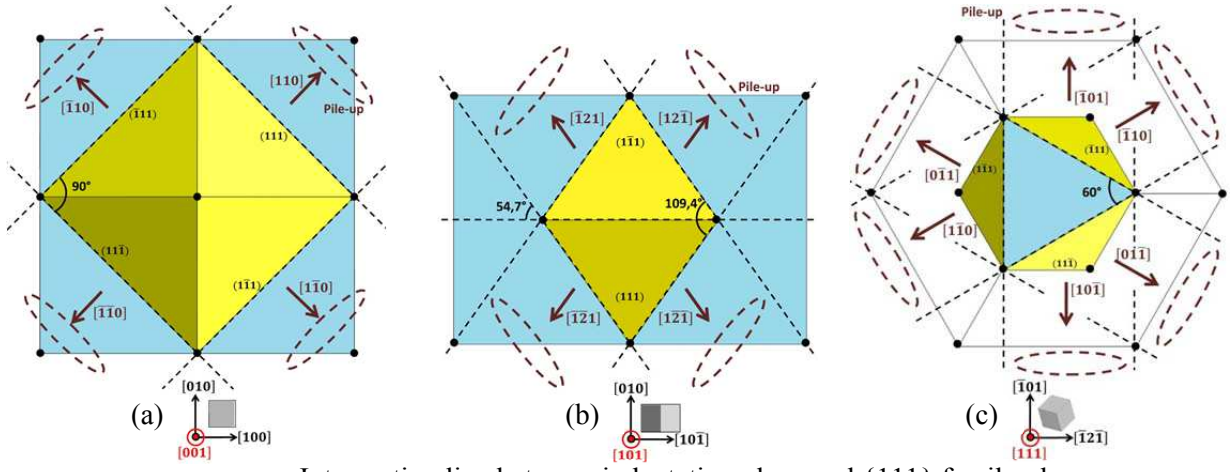

FIG. 4 – Theoretical pile-up propagation directions for an axisymmetric indentation in the (001) (a), (101) (b) and (111) (c) indentation plane.

These theoretical remarks are now compared to the numerical and experiments results. Figures 5a, 5d and 5g presents AFM topography measurements of the indented surfaces (001), (101) and (111), respectively. Figures 5c, 5f and 5i show the corresponding numerical results. The same color scale is used in order to

easily compare experiments and simulation results. Figures 5b, 5e and 5h, show the derivative of the same experimental measurement (with respect to Figures 5a, 5d and 5g), allowing the observation of pile-up (red lines) and sinking-in (green lines) slip lines.

One can notice that from one indentation direction to another, the orientation and/or the number of pile-up show symmetries: four-fold, two-fold for the (001) and (101) orientations, respectively. Concerning the (111) orientation, measurements show a formation of pile-up which presents a three-fold symmetry instead of the expected six-fold symmetry. This phenomenon may result from the Berkovich geometry of the indenter tip. Indeed, the stress field generated by the indenter tends to confine pile-up in front of the indenter faces and in the propagation directions established previously. It is also observed that pile-up dimensions (height and width) are not symmetric. Although these dimensions differ between numerical and experimental results, one can notice the similarities concerning the pile-up propagation directions. A quantitative study will be further carried out with appropriate model parameters for the annealed Ni material.

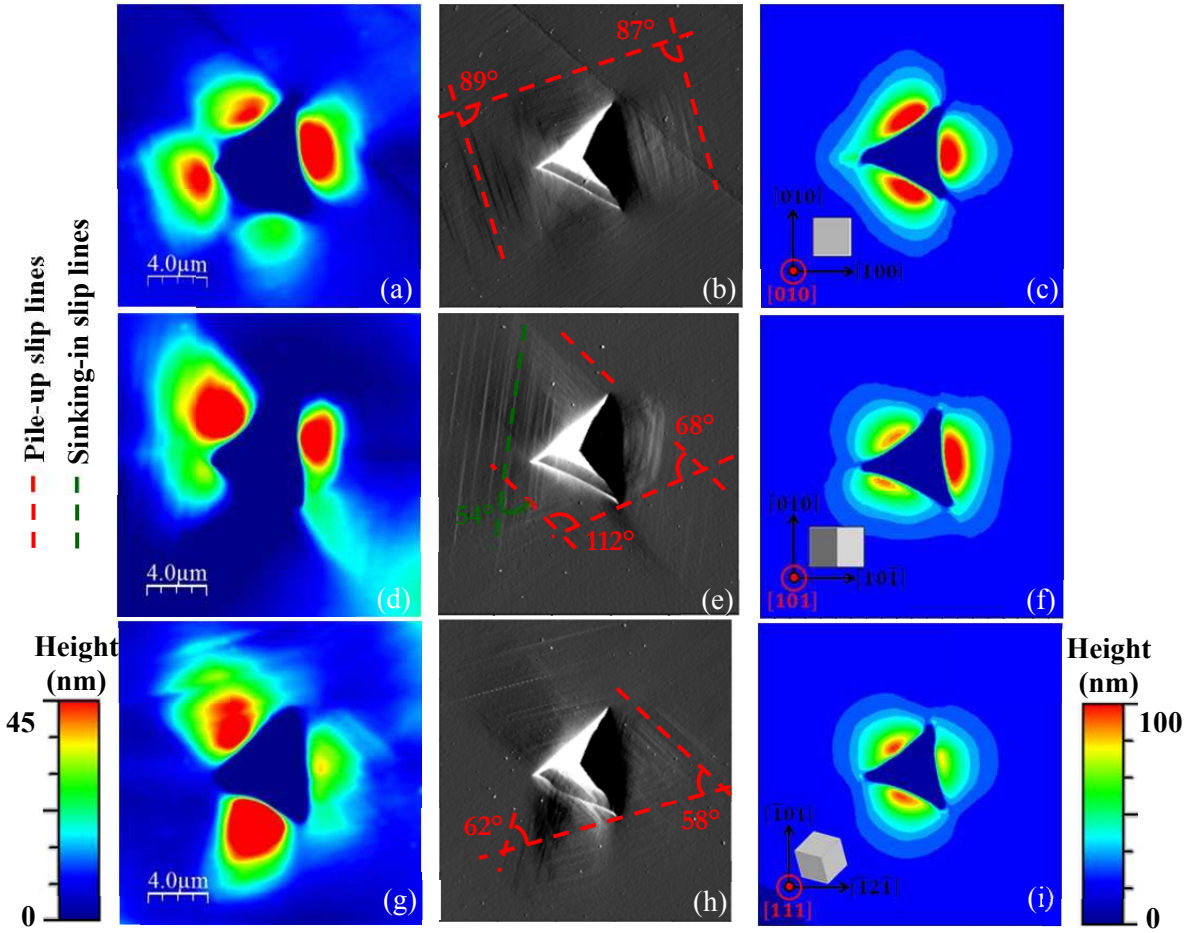

FIG. 5 – Numerical and experimental indentation results in the (001) (a, b, c), (101) (d, e, f) and (111) (g, h, i) indentation planes. AFM Topography measurements: pile-up measurements (a, d, g); slip traces on surface bulk (b, e, h). Numerical topography results (c, f, i).

Indenter orientation effects for (101) indentation plane were also analyzed. Figure 6 shows numerical and experimental indentation results when the indenter is rotated of 30° and 60°. It can be noticed that the indenter rotations have no effect on the pile-up propagation directions. The slip traces at the surface are not distorted and keep the same orientation while the piles-up distribution and above all their dimensions appear to be strongly affected by the rotation. It is worth noting that simulation and experiments show the same tendency.

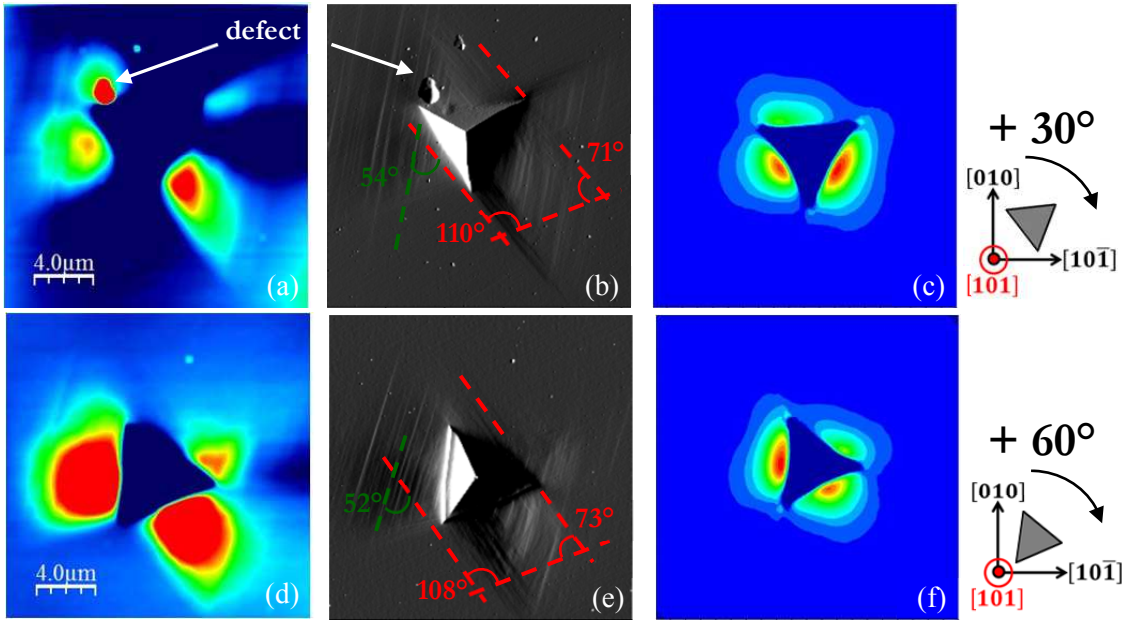

FIG. 6 – Numerical and experimental results after rotating the indenter of 30° (a, b, c) and 60° (d, e, f) in the (101) indentation plane. AFM Topography measurements: Pile-up measurements (a, d); Slip traces on surface bulk (b, e). Numerical topography results (c, f).

5 Conclusions

Nanoindentation measurements were performed on polycrystalline nickel sample, in several large grains characteristic orientations. Material anisotropy and plasticity informations have been obtained through the pile-up analysis. Their propagation directions strongly depend on the material crystallographic orientation under indentation and the stress field generated by the indenter. The nanoindentation test on single crystal can be well simulated using a 3D finite element modeling containing the crystal plasticity constitutive equations. Numerical and experimental results are in a good qualitative agreement. A quantitative study requires the nickel material parameters to be clearly identified. Conical indentations should also be considered in order to clarify the exact role of Berkovich shape in the matter flow distribution, particularly for the (111) indentations.

References

[1] Holmes D., Dislocation structures around Vickers indents in 9.4mol% Y_2O_3-stabilized cubic ZrO_2 single crystals, Philo. Mag.. A, 67, 325-342, 1993.
[2] Stelmashenko N.A., Microindentations on W and Mo oriented single crystals: an STM study, Acta Metall. Mater., 41, 2855-2865, 1993.
[3] Nibur K.A., Identifying slip systems around indentations in fcc metals, Scripta Mat.49, 1055-1060, 2003.
[4] McElhaney K.W., Determination of indenter tip geometry and indentation contact area for depth-sensing indentation experiments, J. Mater. Res., 13, 1300-1306, 1998.
[5] Wang Y., Orientation dependence of nanoindentation pile-up patterns and of nanoindentation microtextures in copper single crystals, Acta Mat., 52, 2229-2238, 2004.
[6] Liu Y., Orientation effects in nanoindentation of single crystal copper, Int. J. Plast., 24, 1990-2015, 2008.
[7] Casals O., Finite element crystal plasticity analysis of spherical indentation in bulk single crystals and coatings, 45, 774-782, 2009.
[8] Zambaldi C., Plastic anisotropy of c-TiAl revealed by axisymmetric indentation, 58, 3516-3530, 2010.
[9] Eidel B., Crystal plasticity finite-element analysis versus experimental results of pyramidal indentation into (001) fcc single crystal, Acta Mat., 59, 1761-1771, 2011.
[10] Hill R., Constitutive analysis of elastic-plastic crystals at arbitrary strain, J. Mech Phys Solids, 20, 401-413, 1972.
[11] Méric L., Single crystal modeling for structural calculations: part 1-Model presentation, J. Eng. Mater. Technol., 113, 162-170, 1991.